JOURNAL OF MATERIALS SCIENCE **36** (2001) 2691 – 2705

Numerical simulation of bubble growth in expanding perlite

K. ZÄHRINGER, J.-P. MARTIN, J.-P. PETIT
Laboratoire d'Energétique Moléculaire et Macroscopique, Combustion, UPR 288 du CNRS, Ecole Centrale Paris, 92295 Châtenay-Malabry Cedex, France
E-mail: zaehringer@em2c.ecp.fr

Aiming to improve the comprehension of the expansion process of perlite, a numerical study has been carried out, concerning the water vapour bubble growth in softened perlite melt. The physical properties of the melt and temperature history during the expansion process are varied, in order to determine the most influencing parameters. Calculated bubble growth results are compared to experimental data obtained in a previous study, and to industrial expansion results. An extensive literature review has been done to determine the physical properties of raw and expanded perlite, as input values to the numerical model.

Nomenclature

A	=	surface, m^2
c_p	=	specific heat, J/(kg K)
D	=	diffusion coefficient, m^2/s
d_p	=	particle diameter, m
E_a	=	activation energy, J/(K mol)
H	=	enthalpy, J
K_h	=	Henry coefficient, Pa^{-1}
m	=	mass, kg
M	=	molar mass, kg/mol
$\dot{m}$	=	mass flux, kg/(s m^2)
n	=	Henry constant, −
p	=	pressure, Pa
$\dot{q}$	=	surface heat flux, W/m^2
r	=	radial distance, m
R	=	radius of the gas bubble, m
$\mathcal{R}$	=	universal gas constant, J/(K mol)
S	=	radius of the cell, m
t	=	time, s
T	=	temperature, K
u	=	growth velocity, m/s
V	=	volume, m^3
X_i	=	mole fraction, −
Y_i	=	mass fraction, −

Greek letters

λ	=	heat conductivity, W/(m K)
μ	=	dynamical viscosity, kg/(m s)
$\mu\Phi$	=	viscous dissipation, Pa
ρ	=	density, kg/m^3
σ	=	surface tension, N/m

Indices

0	=	at $t = 0$
amb	=	ambient
g	=	gas
l	=	liquid
p	=	particle
r	=	radial component
R	=	at radius R
raw	=	raw

1. Introduction

Perlite, a naturally occurring volcanic glass, is used in its expanded form as a granular thermal and phonically insulating material especially in the building industry. Its principal advantages compared to other insulating materials are its lightweight and fire resistant properties. In the last few years perlite has been used for new applications in plasterboards and mortars. Perlite is used in these materials to get a higher fire resistance, better insulating properties and an easier handling due to its lighter weight. These new applications have created a new demand concerning the properties of expanded perlite, especially its granulometry and morphological aspect. Very small particles with well-controlled size distributions and high mechanical stability are needed for these applications. For the most delicate applications small particles of hollow spherical shape consisting of a single bubble are the most required, since they are mechanically resistant, easy to apply and insulating as well.

Perlite gets its insulating properties by an expansion process, which increases the particle diameter to about 3 times its initial value. This expansion is due to the presence of 2 to 6% of combined water in the crude rock. When the raw material is heated to a suitable point in its softening range (between 800–1100°C), the water recombines, vaporises and the steam expands the softened material, thus creating a foamy structure and decreasing the original density and heat conductivity.

Industrial expansion of perlite is done in big rotative or vertical furnaces, which are generally not optimised for the production of the perlite qualities necessary for the new applications. For the production of these qualities the industrial expansion process has to be adapted and a better comprehension of the expansion phenomenon is necessary.

A previous morphological study [1] has shown the foamy structure of expanded perlite. The foam cells of perlite consist of pentaedric or hexaedric faces and correspond to most of the naturally occurring foams [2]. Expansion of perlite is due to the formation and growth of these bubbles in the softened material and a better comprehension of the bubble growth process could give more informations about the expansion phenomenon of perlite.

In this study we developed a numerical model describing the growth of water vapour bubbles in perlite melt. The model supposes that bubble growth is due to water diffusion from the melt to an existing bubble nucleus. The model does not treat bubble formation, coalescence or break-up problems, as well as the creation of microcracks, necessary for expansion.

By varying the physical model parameters like temperature, viscosity or diffusion coefficient, the importance of these parameters for the expansion process can be examined. An extensive literature review concerning the physical properties of perlite had been necessary to determine these input parameters correctly. The calculation results are compared to experimental data obtained from industrially expanded perlite.

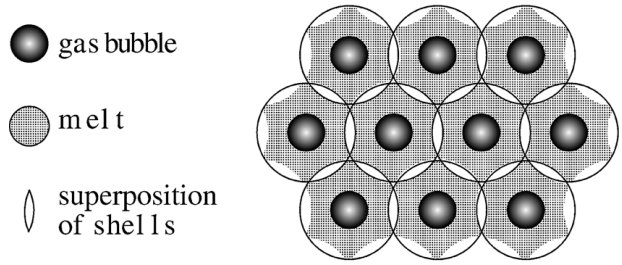

Figure 1 Cellular foam model.

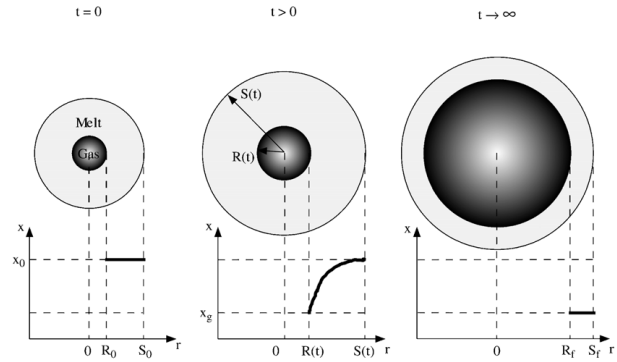

Figure 2 Bubble growth in a finite melt volume.

2. Foam growth model

The foam growth model used in this study is based on the assumption that the foam consists of elementary spherical bubble cells (cell model). The growth of one bubble in a finite volume of liquid (melt) is simulated and considered to be representative for the behaviour of the foam.

This kind of model has been developed by Arefmanesh and Advani [3–7] and is currently used to simulate polymeric foams. Proussevitch and colleagues [8–12] have adapted these models for the simulation of magmatic foams in order to explain volcanic eruptions. They included thermal effects of the volatile evaporation and accounted for the interactions of melt properties such as viscosity and diffusivity.

We used their numerical code to simulate bubble growth during the expansion of perlite. Physical properties, time and pressure scales had to be adapted to those of perlite. Especially we introduced different temperature and composition dependend viscosity and diffusivity calculation methods.

The cells of the model foam consist of a spherical gas bubble surrounded by a finite volume of liquid, in which a volatile component is dissolved (Fig. 1). In the case of perlite expansion, the volatile is water, the liquid is the perlitic melt. Bubble nucleation is not taken into account, the initial bubble size is chosen to be larger than the critical size, necessary to allow growth (see Equation 9). The bubbles are assumed to be independent and no drainage or coalescence are taken into account. Thus it will be sufficient to consider the growth of only one bubble, representative for the whole system.

Bubble growth is supposed to be induced by diffusion of the volatile from the melt to the bubble. Initially the volatile, is distributed uniformly in the melt (Fig. 2 left). During bubble growth, the volatile diffuses in the melt and a concentration profile (defined in terms of molar fraction X on Fig. 2 center) is established inside the melt. The bubble grows until equilibrium between the pressure inside the bubble and the oversaturation level of the melt (Fig. 2 right). We suppose that the outer surface of the cell S is not permeable to the volatile and that there are no external constraints.

Initially the system is isothermal, the external boundaries are adiabatic. During expansion of the gas bubble, a temperature profile is established due to the latent heat of evaporation of water, cooling due to expansion work, viscous heating and conduction inside the melt shell.

2.1. Model equations

The complete derivation of the model equations can be found in [8]. Here only the main assumptions and equations will be summarised. The equations are derived for a spherical symmetry with its origin in the center of the bubble. The main assumptions are :

- the bubble is spherical with an initial gas bubble radius R_0 bigger than the critical growth radius and an initial melt shell radius S_0,
- growth is only due to the diffusion of water, initially uniformly distributed in the melt, coalescence and external forces are neglected,
- the gas inside the bubble is considered as a perfect gas,

- the gas is always in themodynamical equilibrium at the bubble interface,
- the outer surface is not permeable for the gas,
- the system is adiabatic,
- the melt is considered as incompressible and Newtonian.

2.1.1. Continuity equation of the liquid phase

The continuity equation for the liquid in a spherical symmetry and at constant density ρ_l of the melt can be written as:

$$\rho_\mathrm{l}\frac{\partial}{\partial r}\left(r^2 u_r\right) = 0 \tag{1}$$

which is the same as:

$$r^2 u_r = \text{ const. } = R^2 u_R$$

with the growth velocity u_R of the bubble radius R.

2.1.2. Momentum equation

In spherical coordinates, the momentum equation for an incompressible melt, a unidirectional problem and when neglecting gravity effects becomes:

$$\rho_\mathrm{l}\left(\frac{\partial u_r}{\partial t} + u_r\frac{\partial u_r}{\partial r}\right) = -\frac{\partial p}{\partial r} + 2\frac{\partial u_r}{\partial r}\frac{\partial \mu(r)}{\partial r} + 2\mu(r)\frac{\partial^2 u_r}{\partial r^2} + \frac{4}{r}\mu(r)\left(\frac{\partial u_r}{\partial r} - \frac{u_r}{r}\right) \tag{2}$$

with boundary conditions

$$p(R) - p_\mathrm{g} = \tau_\mathrm{rr}(R) - \frac{2\sigma}{R} = 2\mu(R)\frac{\partial u_r}{\partial r}\bigg|_R - \frac{2\sigma}{R} = -4\mu(R)\frac{u_R}{R} - \frac{2\sigma}{R} \quad \text{for} \quad r = R \tag{3}$$

and

$$p(S) - p_\mathrm{amb} = \tau_\mathrm{rr}(S) = 2\mu(S)\frac{\partial u_r}{\partial r}\bigg|_S = -4\mu(S)\frac{R^2 u_R}{S^3} \quad \text{for} \quad r = S \tag{4}$$

where τ_rr is the radial component of the tensor of constraints. By integrating Equation (2) between the gas bubble radius R and the outer cell radius S, introduction of the boundary conditions (3) and (4) and the continuity Equation (1), the momentum equation becomes:

$$p_\mathrm{g} - p_\mathrm{amb} = \frac{2\sigma}{R} - 12R^2 u_R\int_R^S \frac{\mu(r)}{r^4}\,\mathrm{d}r + \rho_\mathrm{l} R\frac{\partial u_R}{\partial t}\times\left(1 - \frac{R}{S}\right) + \rho_\mathrm{l} u_R^2\left(\frac{3}{2} + \frac{1}{2}\frac{R^4}{S^4} - \frac{2R}{S}\right) \tag{5}$$

For highly viscous fluids the two last terms of this equation can be neglected and the momentum equation is written as:

$$\boxed{p_\mathrm{g} - p_\mathrm{amb} = \frac{2\sigma}{R} - 12R^2 u_R\int_R^S \frac{\mu(r)}{r^4}\,\mathrm{d}r} \tag{6}$$

2.1.3. Diffusion equation and mass balancy at the interface

In spherical coordinates the diffusion of the volatile in the melt at constant density ρ_l and written in terms of mass fractions Y is defined by :

$$\boxed{\frac{\partial Y(t,r)}{\partial t} + u_r\frac{\partial Y(t,r)}{\partial r} = \frac{1}{r^2}\frac{\partial}{\partial r}\left(Dr^2\frac{\partial Y(t,r)}{\partial r}\right)} \tag{7}$$

with boundary conditions :

$$\begin{aligned} Y(r,0) &= Y_0 && \text{for} \quad r > R \quad \text{and} \quad t = 0\\ \left(\frac{\partial Y}{\partial r}\right)_{r=S} &= 0 && \text{for} \quad t > 0\\ Y(R,t) &= Y_R = (K_\mathrm{h} p_\mathrm{g})^{1/n} && \text{for} \quad r = R \quad \text{and} \quad t > 0 \end{aligned} \tag{8}$$

The Henry constant K_h is considered to be $n = 2$ for water in silicate melts [13, 14]. The last equation also describes the necessary condition for a bubble to grow. The bubble pressure p_g has to be smaller than the saturation pressure p_sat:

$$p_\mathrm{sat} = \frac{Y_0^2}{K_\mathrm{h}} > p_\mathrm{g} = p_\mathrm{amb} + \frac{2\sigma}{R_0} \quad \text{for} \quad t = 0$$

The initial radius R_0 of the bubble thus has to be larger than the critical bubble radius R_crit to allow bubble growth.

$$R_0 > R_\mathrm{crit} = \frac{2\sigma}{\frac{Y_0^2}{K_\mathrm{h}} - p_\mathrm{amb}} \quad \text{for} \quad t = 0 \tag{9}$$

The mass balancy at the bubble interface ($r = R$) can be written as:

$$\frac{\mathrm{d}m_\mathrm{g}}{\mathrm{d}t} = \frac{\mathrm{d}}{\mathrm{d}t}(V_\mathrm{g}\rho_\mathrm{g}) = \frac{\mathrm{d}}{\mathrm{d}t}\left(\frac{4}{3}\pi R^3\rho_\mathrm{g}\right) = -A\dot{m}_\mathrm{g} = 4\pi R^2 D\rho_\mathrm{l}\frac{\partial Y}{\partial r}\bigg|_{r=R} \tag{10}$$

After introduction of the ideal gas law this equation becomes:

$$\boxed{\frac{\mathrm{d}}{\mathrm{d}t}\left(\frac{p_\mathrm{g}R^3}{T_\mathrm{g}}\right) = 3\frac{\mathcal{R}}{M}R^2 D\rho_\mathrm{l}\frac{\partial Y}{\partial r}\bigg|_{r=R}} \tag{11}$$

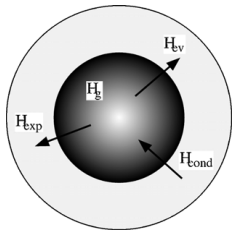

Figure 3 Enthalpies used for the temperature determination in the gas bubble.

2.1.4. Energy equations

For the energy conservation inside the gas bubble we take into account the gas enthalpy H_g, cooling due to volatile evaporation H_{ev}, cooling due to bubble expansion H_{exp} and the heat flux from the surrounding melt H_{cond} (Fig. 3):

$$dH_g + dH_{ev} + dH_{exp} = dH_{cond}$$

We also suppose that the gas temperature T_g only depends on time. Gas enthalpy is defined by:

$$\begin{aligned} dH_g &= m_g c_{p_g} dT_g = V_g \rho_g c_{p_g} dT_g \\ &= \frac{4}{3}\pi R^3 \frac{p_g M}{\mathcal{R} T_g} c_{p_g} dT_g \end{aligned} \quad (12)$$

Heat flux due to expansion of the melt is written as:

$$dH_{exp} = -V_g dp_g = -\frac{4}{3}\pi R^3 dp_g \quad (13)$$

Heat flux due to evaporation depends on the mass flux from the melt to the bubble (Equation 10) and we suppose that the latent heat is delivered by the gas:

$$\begin{aligned} dH_{ev} &= \frac{\Delta H_{ev}}{M} dm_g = \frac{\Delta H_{ev}}{M} A\dot{m} \\ &= \frac{\Delta H_{ev}}{M} 4\pi R^2 \left(D\rho_l \frac{\partial Y}{\partial r}\bigg|_{r=R} \right) dt \end{aligned} \quad (14)$$

with ΔH_{ev} the molar latent heat of evaporation. The conductive heat flux is determined by:

$$dH_{cond} = A\dot{q}_{cond} = 4\pi R^2 \left(\lambda_l \frac{\partial T_g}{\partial r}\bigg|_{r=R} \right) dt \quad (15)$$

Combining Equations 12 to 15, temperature evolution of the gas bubble becomes:

$$\boxed{\frac{\partial T_g}{\partial t} = \frac{3\mathcal{R} T_g}{p_g R c_{p_g} M} \left(\lambda_l \frac{\partial T_g}{\partial t}\bigg|_{r=R} - \Delta H_{ev} \frac{1}{M} D\rho_l \frac{\partial Y}{\partial r}\bigg|_{r=R} + \frac{R}{3}\frac{\partial p_g}{\partial t} \right)} \quad (16)$$

For the heat balancy of the melt we take into account the heat losses due to conduction and heating due to viscous dissipation:

$$\rho_l c_{p_l} \frac{dT_l}{dt} = \text{div}\,(\lambda_l \vec{\text{grad}}\, T_l) + \mu\Phi \quad (17)$$

with:

$$\mu\Phi = 2\mu \left[\left(\frac{\partial u_r}{\partial r} \right)^2 + 2\left(\frac{u_r}{r} \right)^2 \right] \quad (18)$$

By introducing Equation 18 into Equation 17, and by taking into account the continuity equation (1) the temperature of the liquid phase can be written as:

$$\boxed{\frac{\partial T_l}{\partial t} + u_r \frac{\partial T_l}{\partial r} = \frac{1}{r^2}\frac{\partial}{\partial r}\left(r^2 \frac{\lambda_l}{\rho_l c_{p_l}} \frac{\partial T_l}{\partial r} \right) + 12 u_R^2 \frac{\mu}{\rho_l c_{p_l}} \frac{R^4}{r^6}} \quad (19)$$

with boundary conditions:

$$\begin{aligned} &T_l(r, 0) = T_0 \quad \text{for} \quad r \geq R \quad \text{and} \quad t = 0 \\ &\left(\frac{\partial T_l}{\partial r} \right)_{r=S} = 0 \quad \text{for} \quad t > 0 \\ &T_l(R, t) = T_g \quad \text{for} \quad r = R \quad \text{and} \quad t > 0 \end{aligned} \quad (20)$$

Equations 6, 7, 11, 16 and 19 constitute the system of governing equations of the bubble growth problem.

In order to resolve this system of equations we used the numerical code developed by Proussevitch, Sahagian et Anderson [8] for applications in magmatic foams and adapted it to the case of expanding perlite, by introducing the appropriate calculation methods for its physical properties.

3. Physical properties of perlite

In order to introduce the physical properties of perlite into the above bubble growth model, an extensive literature review has been necessary. The physical properties of expanded perlite are rather well examined in literature, those of raw perlite are very poorly known. Therefore we also paid attention to the physical properties of materials similar to perlite (volcanic and commercial glasses, magma). The temperature range in industrial expansion being rather large (ambient to 1300°C), the physical properties had to be determined for this whole range to get representative results.

3.1. Density

Literature values for the density of perlite melt vary from 2200 to 2400 kg/m^3 [15–17]. Murase and McBirney [18] have measured the density of an obsidian melt between 800 and 1250°C. In this temperature range density does not change significantly and is situated around 2200 kg/m^3. In our calculations we used a mean value of 2350 kg/m^3.

3.2. Viscosity

Viscosity plays a key role in the expansion process of perlite. Its determination in function of the temperature and chemical composition will strongly influence calculation results. In the temperature range encountered during expansion, viscosity changes by more than ten orders of magnitude.

Water content of the melt has the strongest influence on viscosity values. A decrease of one order of magnitude per percentage of water content is generally supposed [19, 20]. Friedman *et al.* [20] also stated that the influence of temperature on the viscosity decreases with increasing water content. They obtained viscosity values of $10^{13.5}$ Pa · s to $10^{8.5}$ Pa · s for rhyolitic glasses between 350 and 850°C and water contents of 0.1 to 3%. Murase and McBirney [18] determined the viscosity of obsidian with 0.5% water between 600 and 1300°C and obtained values of 10^{14} to 10^{5} Pa · s.

Oxides like Na_2O, K_2O, Fe_2O_3, TiO_2, CaO and MgO also decrease the viscosity of the melt, but their influence is much less than that of water. Aluminium oxide has an inverse effect: it increases the viscosity of the melt and thus inhibits expansion of perlite. This can be seen on perlite production sinks consisting in materials containing less water, Na_2O and K_2O, but more Al_2O_3, Fe_2O_3 and TiO_2 [21].

Due to the importance of melt viscosity for volcanic erruptions and in the glass industry, different calculation methods exist for the determination of viscosity in function of temperature and chemical composition [22]. In general they are based on an Arrhenius equation for the temperature dependency. The activation energies and preexponential factors are determined in function of the composition.

In our study we specially used the methods of Bottinga and Weill [23], improved by Shaw [24] and a non-arrhenian method of Hess and Dingwell [25]. These methods have been developed for the determination of magma viscosities.

In their empirical model, Bottinga and Weill [23] and finally Shaw [24] are representing the viscosity μ in function of the molar composition X_i as:

$$\ln \mu = \sum X_i \cdot \ln \mu_i \tag{21}$$

Temperature influence is described by an Arrhenius equation:

$$\mu = \mu_o \exp\left(\frac{E_a}{\mathcal{R}T}\right) \tag{22}$$

which is linearised as:

$$\ln(\mu[\text{Poise}]) = s(10^4/T[K]) - c_T s + c_\mu \tag{23}$$

where s represents the slope of the natural logarithm of the viscosity of the multicomponent mixture in function of the inverse temperature. The slope value s is determined from the partial slope values s_{i0} of the pseudobinary system between SiO_2 and the constituent oxides. The partial slope values s_{i0} for $X_{SiO_2} = 1$ represent characteristic values for each oxide and are given in Table I.

TABLE I Characteristic partial slope values s_{i0} for viscosity calculations, Shaw [24]

	s_{i0} K	Corresponding molar activation energy kcal/mol
H_2O	2.0	40
K_2O, Na_2O, Li_2O	2.8	56
MgO, FeO	3.4	68
CaO, TiO_2	4.5	89
AlO_2	6.7	134

The mean values of c_T and c_μ for magmatic melts are $c_T = 1.50\ K^{-1}$, $c_\mu = -6.40$ [24].

The total slope value s in Equation 23 is calculated from these values by multiplying them with the molar fraction of the corresponding oxide, summing them up and dividing by the molar fraction of the other oxides. Viscosity then can be calculated with Equation 23, temperature dependency with Equation 22.

The authors underline that this method only should be used for viscosities smaller than 10^7 Pa · s, the softening point of glass. Very high water contents (>6% of mass) or high pressure (>1000 bar) can lead to wrong viscosity calculations.

Hess and Dingwell [25] use a non-arrhenian approach to calculate magma viscosities. Their empirical method is based on the analysis of experimental results published by different authors. These include water contents Y_{H_2O} of 0.02 to 12.3% and temperatures between 610 and 1916 K. Hess and Dingwell finally propose an equation to represent these experimental results for granitic and rhyolitic melts:

$$\log \mu = [-3.545 + 0.833 \ln(Y_{H_2O})] + \frac{9601 - 2368 \ln(Y_{H_2O})}{T[K] - [195.7 + 32.25 \ln(Y_{H_2O})]}$$

The influence of the metallic oxides is considered to be negligible compared to the influence of the water content.

The results obtained by the two methods for a typical perlite composition with 3% water (see Table III) are represented on Fig. 4. Below 600 K, the method of Hess and Dingwell predicts much higher viscosities than the method of Shaw. Between 600 and 1500 K the viscosities of Shaw are up to two orders of magnitude higher than those of Hess et Dingwell (logaritmic scale on Fig. 4). On the same figure we also represented the viscosity of the same perlite but without water, calculated with Shaw's method.

Both methods are widely used in literature and validated for different natural glasses by experimental measurements [23–25]. For numerical calculations, the method of Hess and Dingwell may cause problems, since the logarithm of the viscosity tends to $-\infty$ when approaching zero mass fraction of water. For that reason we generally used Shaw's method, which showed in our test calculations a good agreement compared to experimental literature values for viscosity [18, 23–27].

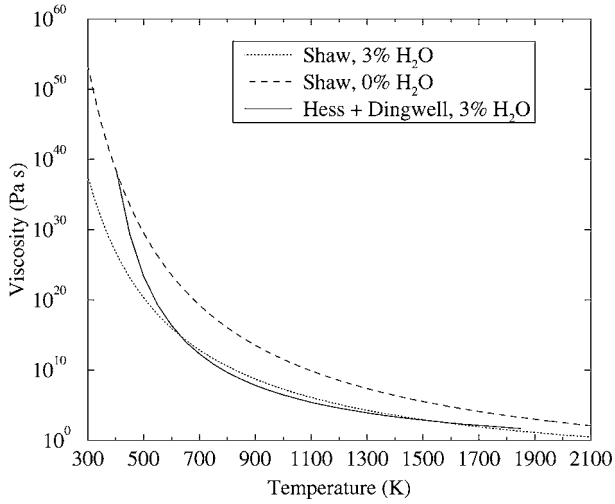

Figure 4 Perlite viscosity calculated with the methods of Shaw [24] and Hess and Dingwell [25].

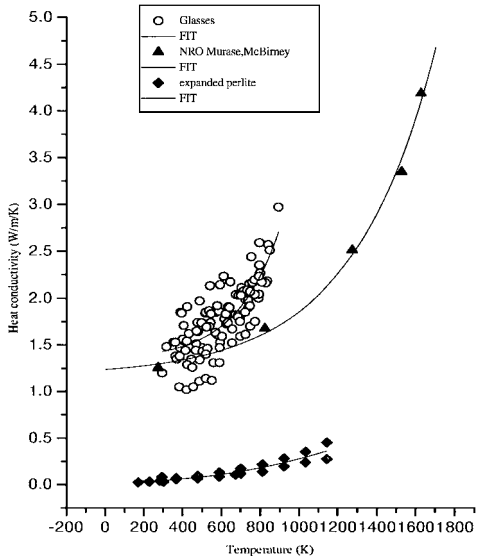

Figure 5 Heat conductivity of expanded perlite ♦ [15, 17], and analogous non-expanded materials (glasses ○ [29] and obsidian [18]).

3.3. Heat conductivity

Heat conductivities of expanded perlite are well known in the literature (e.g. [15, 17]) due to its insulation applications. These values cover a temperature range from 150 to 1150 K (Fig. 5, losanges ♦) for heat conductivity values λ between 0.025 and 0.45 W/(m K). To use these values in our numerical calculations, we interpolated them with the following equation:

$$\lambda\left[\frac{\mathrm{W}}{\mathrm{mK}}\right] = 0.0433918 - 0.806781 \times 10^{-4}\, T[K] + 0.313595 \times 10^{-6}\, T^2[K] \qquad (24)$$

These values also correspond to values measured for Little Glass Mountain obsidian foams by Bagdassarov and Dingwell [28].

As to our knowledge there are no literature values for raw perlite heat conductivity. Touloukian [29] gives heat conductivities of different glasses, represented on Fig. 5 by circles ○. Murase and McBirney [18] determined the heat conductivity of obsidian (Newberry Rhyolite Obsidian) at temperatures from 300 to 1600 K (Fig. 5, triangles). We used these values in our calculations and represented them by:

$$\lambda\left[\frac{\mathrm{W}}{\mathrm{mK}}\right] = 1.173571 + 0.065649 \times \exp(T[K]/427.333981)$$

3.4. Heat capacity

This property has been examined in detail by King, Todd and Kelley [30]. They determined the heat capacity C_p of different perlite qualities with various water contents. For fully dehydrated perlite (Fig. 6, bold line) their regression equation in function of temperature T is:

$$C_\mathrm{p}(0\%\,\mathrm{H_2O})\left[\frac{\mathrm{J}}{\mathrm{kgK}}\right] = (24.25 + 4.66 \times 10^{-3} T[K] - 6.62 \times 10^{5} T^{-2}[K]) \times 41.868 \qquad (25)$$

The heat capacity of perlites containing water is always higher than these values, but the authors don't give indications how to calculate the heat capacity in these cases. Perlite expanders give a value of 837 J/(kg K) at ambient temperature [15].

Bacon [31] developed a method for calculating the heat capacity of glasses from their chemical composition. For a typical perlite composition these values are represented on Fig. 6 by a fine solid curve. These values are smaller than the values of King *et al.* The presence of water can not be taken into account with this method.

In order to represent the influence of the water content of raw perlite, we decided to add the heat capacity $C_\mathrm{p}(\mathrm{H_2O})$ of water vapour in function of its mass fraction $Y(\mathrm{H_2O})$ to the heat capacity of dehydrated perlite:

$$C_{\mathrm{p_{perl}}} = (1 - Y(\mathrm{H_2O}))\cdot C_\mathrm{p}(0\%\,\mathrm{H_2O}) + Y(\mathrm{H_2O})\cdot C_\mathrm{p}(\mathrm{H_2O})$$

The results of this calculation are represented by a dotted curve on Fig. 6 for a water mass fraction of 3%. The

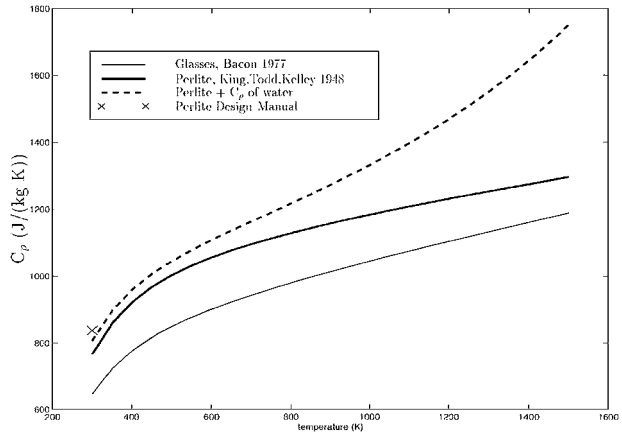

Figure 6 Heat capacity of perlite [15, 30] and glasses [31] in function of temperature.

presence of water has a very strong influence at high temperatures, but at these temperatures perlite would have lost most of its water content and be expanded and Equation 25 has to be used to calculate the heat capacity.

3.5. Surface tension

Murase and McBirney [18] determined the surface tension of obsidian (0.5% water) in a temperature range between 1000 and 1400°C. It shows a linear dependency on temperature (Fig. 7) and can be described by:

$$\sigma = 0.09317 + 1.971 \times 10^{-4} T[^{\circ}\mathrm{C}] \qquad (26)$$

In the temperature range considered, surface tension takes values between 0.29 N/m and 0.37 N/m.

Proussevitch *et al.* [8] use a constant value of 0.32 N/m for their study of bubble growth in rhyolitic magmas. In Equation 26 this corresponds to a temperature of $T = 1150^{\circ}$C.

3.6. Diffusion coefficient

There is much literature concerning water diffusion in natural glasses (e.g. [32–38]). The values given in these references for diffusion coefficients and activation energy are summarised in Table II and Fig. 8.

Moulson and Roberts [33] determined the temperature dependency of the diffusion coefficient of magmatic liquids between 600 and 1200°C and give two equations for its determination :

$$D = 1.0\,(\pm 0.2) \times 10^{-6} \exp\left(\frac{76494\,(\pm 20990)}{\mathcal{R}T}\right) \times 10000\left[\frac{\mathrm{m}^2}{\mathrm{s}}\right] \quad \text{for addition of water}$$

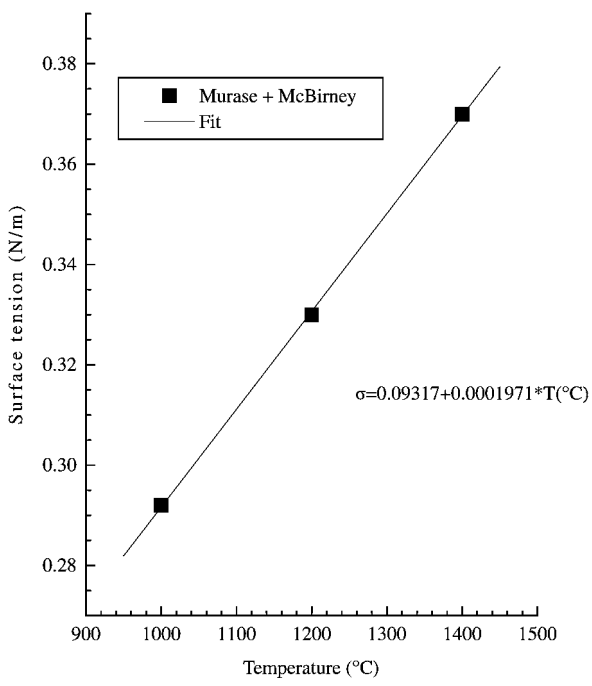

Figure 7 Surface tension of obsidian [18].

TABLE II Diffusion coefficients and activation energies for the diffusion of water in natural and commercial glasses

Author	Temperature	D [m^2/s]	E_a [kJ/mol]
Marshall [32]	20°C	10^{-27}	125.4
Moulson and Roberts [33]			
addition	1000 K	1.7×10^{-10}	76.5
removal	1000 K	4.4×10^{-11}	72.3
Zhang *et al.* [34]	1000 K	1.91×10^{-12}	103
Boulos and Kreidl [35]			
addition	1000°C	7.2×10^{-14}	76.5
removal	1000°C	2.9×10^{-14}	72.3
Friedman *et al.* [36]	-	-	83
Lee [37]	-	-	64.8 - 102.4
Karsten *et al.* [38]	-	-	79.4

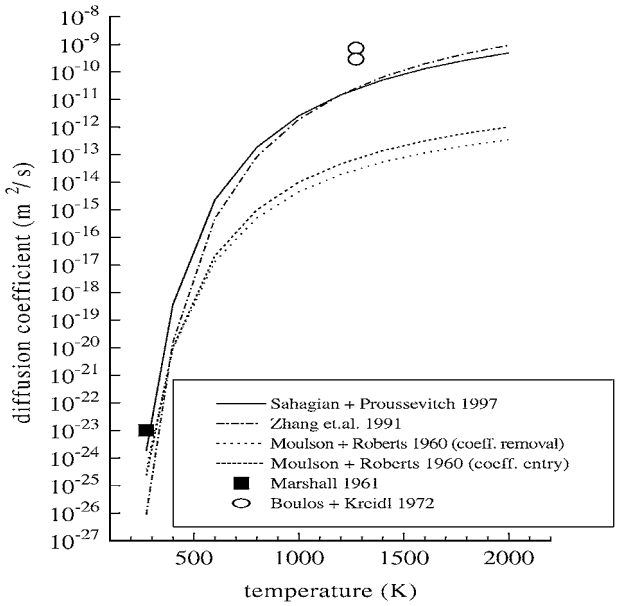

Figure 8 Diffusion coefficients of water in natural glasses.

$$D = 2.7(\pm 1.0) \times 10^{-7} \exp\left(\frac{72314\,(\pm 8360)}{\mathcal{R}T}\right) \times 10000\left[\frac{\mathrm{m}^2}{\mathrm{s}}\right] \quad \text{for removal of water}$$

Zhang *et al.* [34] give an equation for rhyolitic glasses between 673 and 1123 K:

$$\ln D = -14.59\,(\pm 1.59) - \frac{103000\,(\pm 5000)}{\mathcal{R}T} \times \left[D \text{ in } \left(\frac{\mathrm{m}^2}{\mathrm{s}}\right)\right]$$

The results of these equations show a difference of up to 3 orders of magnitude, as it can be seen on Fig. 8 (dotted curves). The diffusion coefficient of Moulson and Roberts is always smaller than the one of Zhang *et al.* In our calculations we used both methods, in order to determine the influence of the diffusion coefficient determination for the expansion process.

4. Numerical results

4.1. Parameter study

In order to validate the foam growth model for the case of perlite, we first tested the influence of the physical properties introduced and presented in the previous section. This also allowed the determination of the most important parameters for the expansion process.

For this study, we used a reference cell with a bubble diameter $R_0 = 4.5\ \mu$m and a cell diameter $S_0 = 17.2\ \mu$m at a temperature of 1000°C. This temperature is a typical furnace temperature in the industrial expansion process. The bubble and cell radius have been calculated from the mean bubble diameter (80 μm) and cell thickness (1 μm) determined experimentally in a previous study [21]. The viscosity has been determinated with the method of Shaw [24], the diffusion coefficient is calculated with the equation of Zhang *et al.* [34].

The raw perlite composition used for this study corresponds to a typical composition of Provatas perlite from the island of Milos in Grece (Table III).

TABLE III Composition of raw perlite used in this study

SiO2	Al2O3	Fe2O3	CaO	MgO	TiO2	Na2O	K2O	H2O
74.7	11.6	1.08	1.29	0.51	0.1	3.65	2.84	3.09

4.1.1. Influence of the initial cell size

The initial bubble radius R_0 and the cell radius S_0 have been varied in a way to keep constant the mass of the melt. Five different combinations have been tested.

R_0 [μm]	14.4	12.3	9.4	7.1	4.5
S_0 [μm]	20	19	18	17.5	17.2

The results of these calculations are represented on Fig. 9. The final bubble radius (125 μm) is the same for all five initial radiuses (Fig. 9 top, left), since it is only determined by the water content. For times smaller than 0.5 s, the bubble radius R is different in the five cases. After this moment the radius is nearly the same and the initial radius has no more influence.

As residence time of the particles in the industrial expansion process is generally in the order of one second, we will have to pay attention to the initial calculation radius for comparison with experimental results.

The mean viscosity of the melt in function of time and different initial radius is represented on the right top of Fig. 9. For bigger cells, viscosity is increasing faster at the beginning of the expansion than for smaller cells. This is due to the bigger surface between the bubble and the melt, which increases the water diffusion and decreases the viscosity of the melt due to the water loss. The final viscosity is the same for all initial cell sizes, since it is determined by the chemical composition and temperature, which are the same in all cases.

Gas pressure inside the bubble increases with decreasing initial bubble size (Fig. 9 bottom, left). Due to the bigger viscosity of the small bubble, the dynamic pressure term of the momentum equation (6) decreases. Ambient pressure can be neglected in our case compared to the much bigger bubble pressures.

The mean temperature of the melt decreases during expansion from 1000°C to 983°C (Fig. 9 bottom, right). This temperature difference is essentially due to the water evaporation inside the bubble.

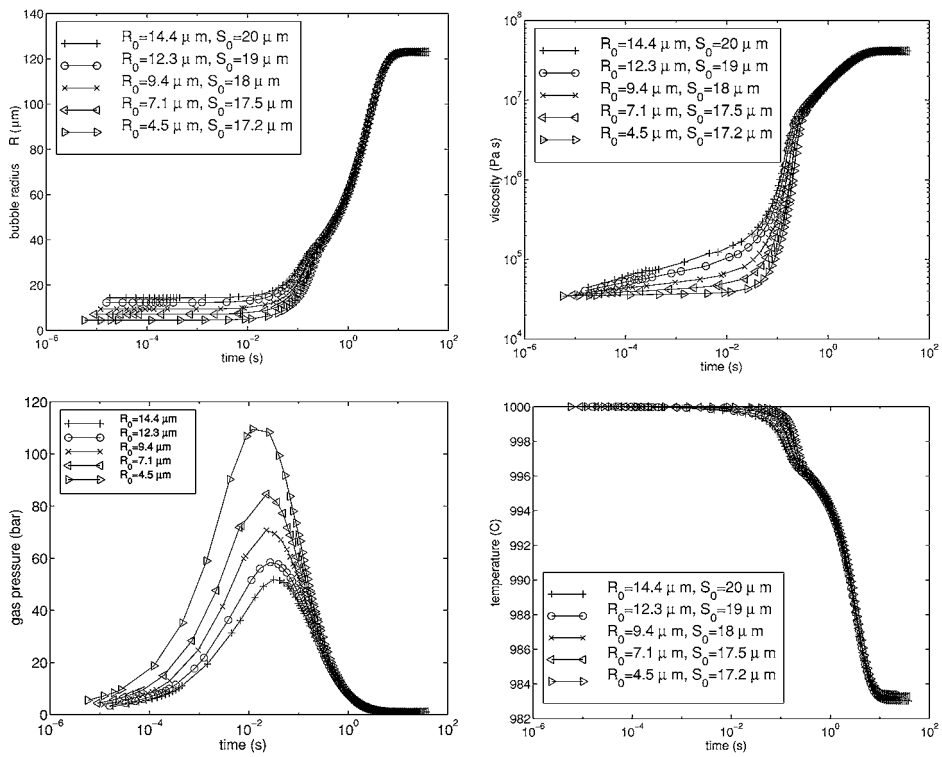

Figure 9 Influence of the initial cell size on bubble growth in perlite: gas bubble radius R (top, left), viscosity (top, right), gas pressure (bottom, left) and mean melt temperature (bottom, right).

4.1.2. Influence of the initial temperature

The influence of the initial temperature on the bubble growth of a cell with $R_0 = 4.5$ μm and $S_0 = 17.2$ μm is represented on Fig. 10. The viscosity has been calculated with Shaw's method, the diffusion coefficient with the equation of Zhang *et al.*

Bubbles are growing faster and to bigger diameters if initial temperature is higher. The reason is the decrease of viscosity of some orders of magnitude, if temperature increases (Fig. 10 top, right). In that case a lower pressure is sufficient to expand the bubble. The final cell radius is slightly bigger if temperature is higher, since the glassy shell is thinner due to the smaller viscosity (Fig. 10 bottom, right).

4.1.3. Influence of the initial water content

The influence of the initial water content of the melt is shown on Fig. 11 for an initial radius $R_0 = 4.5$ μm. Initial temperature is 1000°C, viscosity has been calculated with Shaw's method, the diffusion coefficient with the equation of Zhang *et al.*

When doubling the water mass fraction from 2% to 4%, the final radius is increasing for one third from 106 μm to 136 μm. During the period of strongest growth between 0.1 and 1 second, the diameter of the bubble with 4% of water (symbols "x") can be 8 times bigger than the one of the bubble with 2% of water (symbols "+"). Growth begins later and final bubble radius is reached later for the bubble with less water.

This can be explained by the viscosity of the melt, which is two orders of magnitude smaller for the bubble with 4% water (Fig. 11 top, right), since water is the component with the biggest influence on viscosity.

Pressure is smaller in the cell with 4% water (Fig. 11 bottom, left). The mean temperature of the melt is decreasing faster if water content is high. The latent heat of evaporation is higher in that case and the melt is cooled faster.

4.1.4. Influence of the viscosity

In order to examine the influence of viscosity on the expansion process, two different methods (Shaw [24] and Hess and Dingwell [25]) for calculating the viscosity in function of temperature and chemical composition have been used. The initial radius of the bubble is 4.5 μm, initial temperature 1000°C. The diffusion coefficient is calculated with the equation of Zhang *et al.*

The final bubble radius is the same for both viscosities (Fig. 12 top, left) since equilibrium is attained when all water has diffused to the gas bubble. At the beginning of expansion ($t < 0.05$ s) less water has diffused and the influence of water loss on the calculation of the viscosity is small. During the strongest growth period between $t = 0.05$ s and $t = 5$ s the difference between the bubble radius, obtained with the two methods, is very strong. The radius calculated with the method of Hess and Dingwell can be two times bigger than the

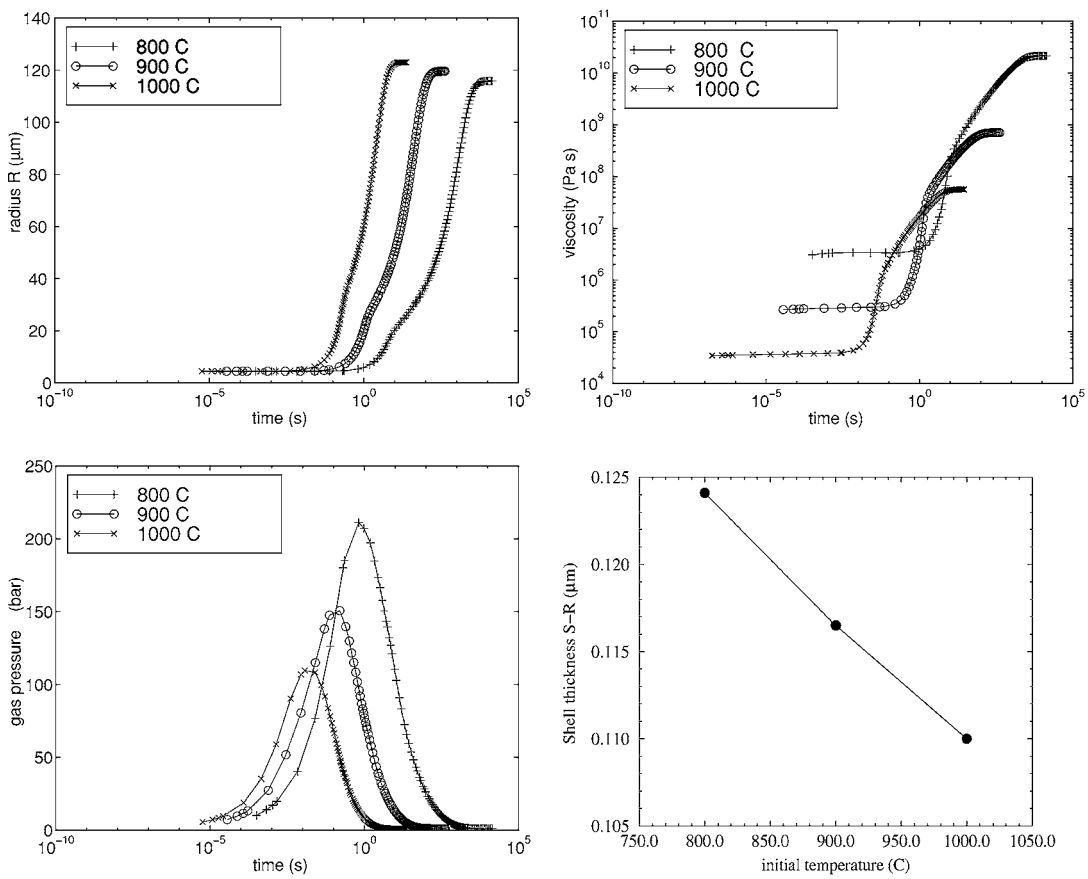

Figure 10 Influence of the initial temperature on bubble growth in perlite: gas bubble radius R (top, left), viscosity (top, right), gas pressure (bottom, left) and shell thickness $S - R$ (bottom, right).

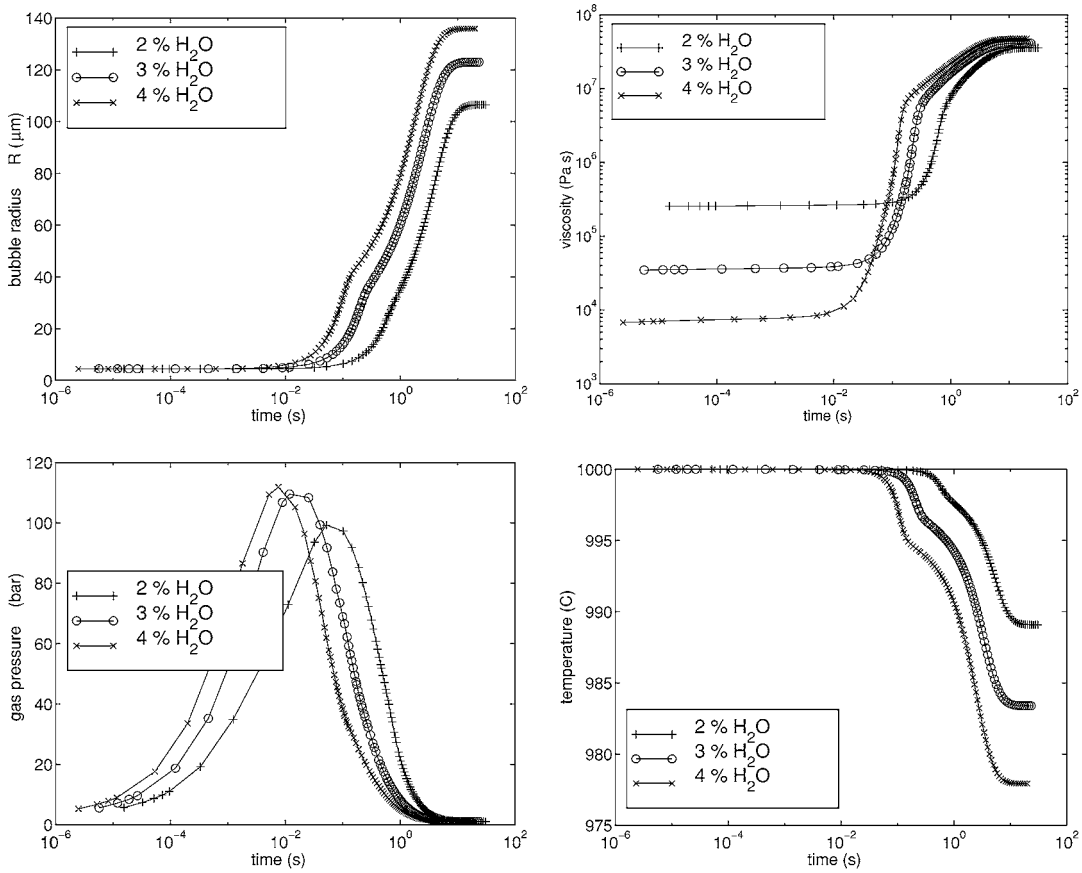

Figure 11 Influence of the initial water content on bubble growth in perlite: gas bubble radius R (top, left), viscosity (top, right), gas pressure (bottom, left) and mean melt temperature (bottom, right).

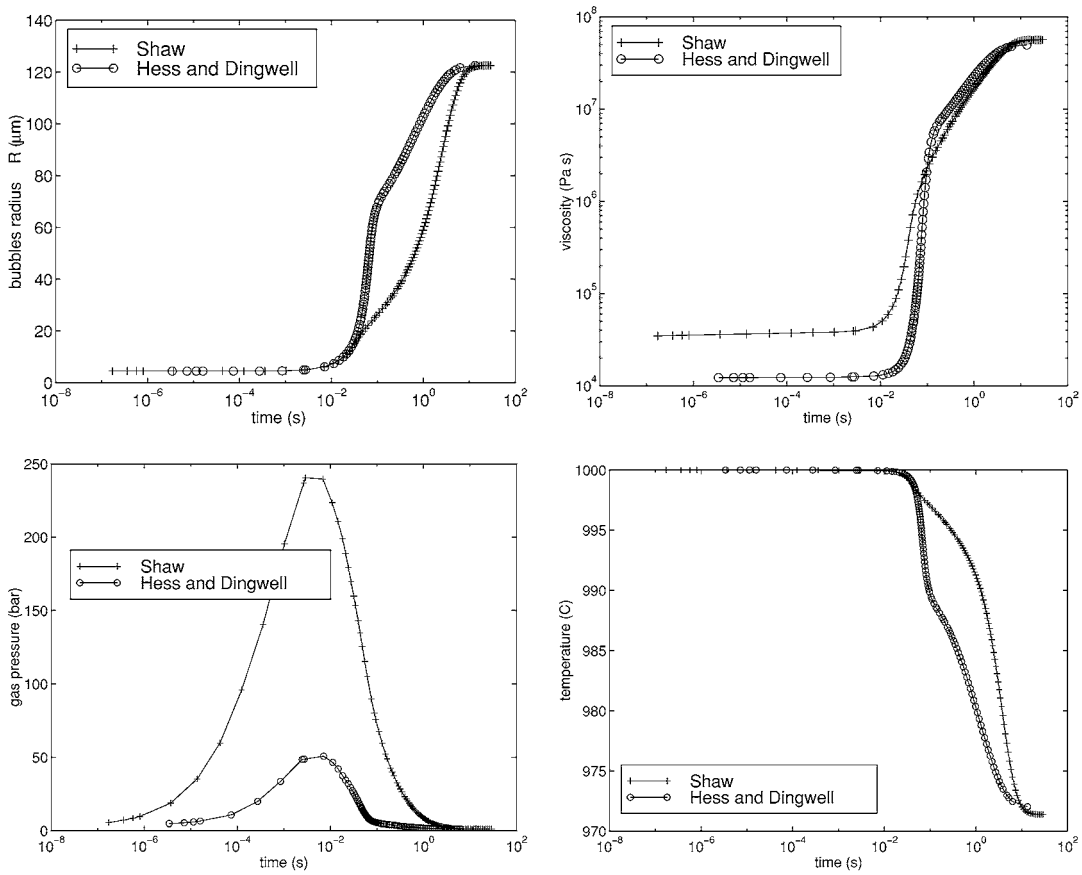

Figure 12 Influence of viscosity calculation method on bubble growth in perlite: gas bubble radius R (top, left), viscosity (top, right), gas pressure (bottom, left) and mean melt temperature (bottom, right).

radius obtained with Shaw's method (Fig. 12 top left, $t = 0.1$ to 1 s).

These results can be explained by the viscosity difference calculated for the same material with the two different methods. Viscosity of Shaw exceeds the viscosity of Hess and Dingwell by up to one order of magnitude. Bubble growth is slower and a higher pressure is necessary to expand the bubble (Fig. 12 bottom, left).

At the beginning, mean temperature of the melt is higher for Shaw's method, since the higher viscosity leads to higher viscous heating (Fig. 12 bottom, right). Final temperature is nearly the same, due to the latent heat of water evaporation, which is the biggest term in the energy equation.

4.1.5. Influence of the diffusion coefficient

The strong differences for the diffusion coefficient of water in natural glasses have been shown in Section 3.6. In order to determine its influence on the expansion process, we compare in this section the results obtained with the coefficients of Moulson and Roberts [33] and those of Zhang *et al.* [34]. Viscosity has been determined by the method of Shaw [24], initial radius is 4.5 μm, initial temperature 1000°C.

The diffusion coefficient has its strongest influence on the bubble radius until $t \approx 2$ s (Fig. 13 top, left). During this time the bubble radius can be up to 4 times bigger if calculated like Zhang *et al.* [34] compared to the diffusion coefficient of Moulson and Roberts [33]. Since industrial expansion takes place during this period, the choice of D is very important for the validity of model calculations.

The bigger diffusion coefficient of Zhang leads to higher viscosity, due to smaller water content (Fig. 13 top, right). Higher gas pressure is necessary to expand the bubble.

The melt is cooled more rapidly (Fig. 13 bottom, right) since higher pressure causes higher heat loss due to expansion (Equation 13).

4.2. Simulation of the bubble growth during perlite expansion in an industrial furnace

In the previous sections, bubble growth has been observed until its maximum diameter when equilibrium has been attained between water concentration in the melt and water vapour pressure in the bubble. During industrial expansion, the perlite particle has a limited residence time in the furnace and is cooled quasi-instantaneously at the exit of the furnace. Bubble expansion thus is stopped immediately. At the same time, particle temperature varies inside the furnace, since particles have to be heated up from injection temperature to expansion temperature.

In order to simulate the bubble size at the exit of an expansion furnace, we have to take into account the temperature evolution of the particle during its trajectory in the furnace and its total residence time.

On Fig. 14 are represented typical particle center (Tp0) and surface temperatures (Tps) for two 1 mm

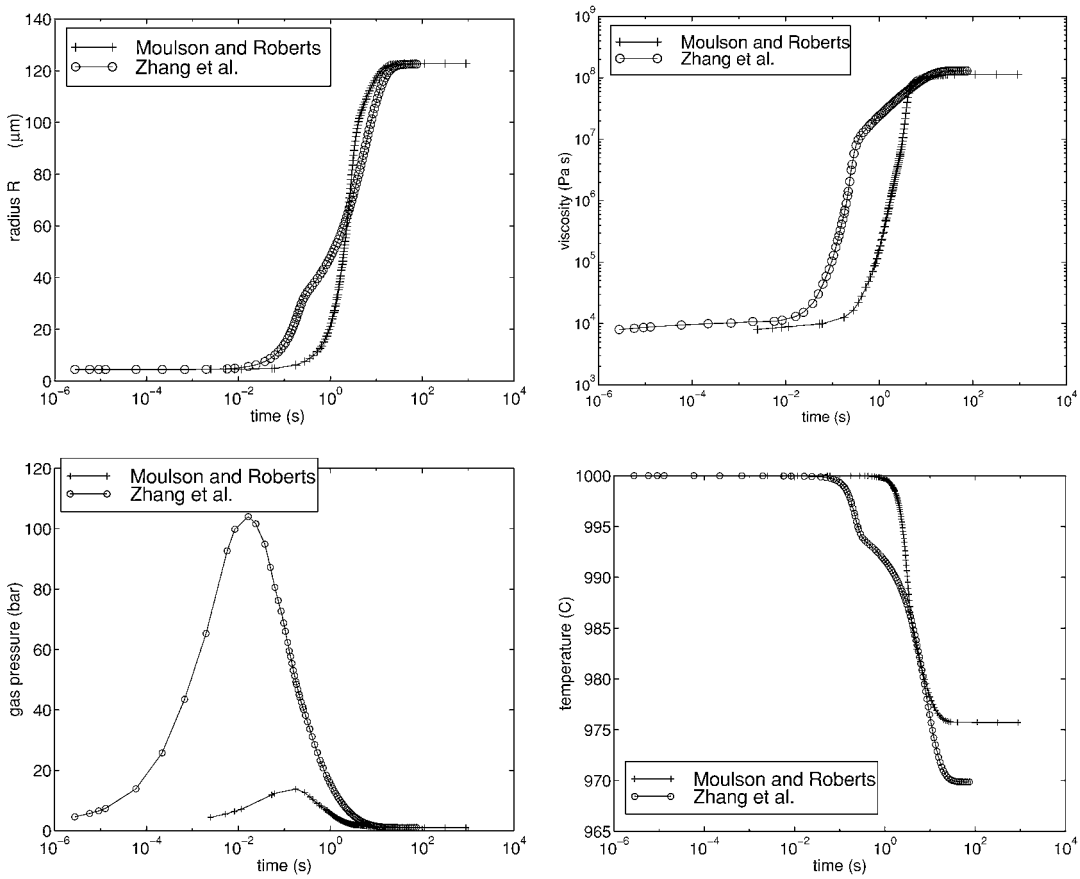

Figure 13 Influence of diffusion coefficient calculation method on bubble growth in perlite: gas bubble radius R (top, left), viscosity (top, right), gas pressure (bottom, left) and melt temperature (bottom, right).

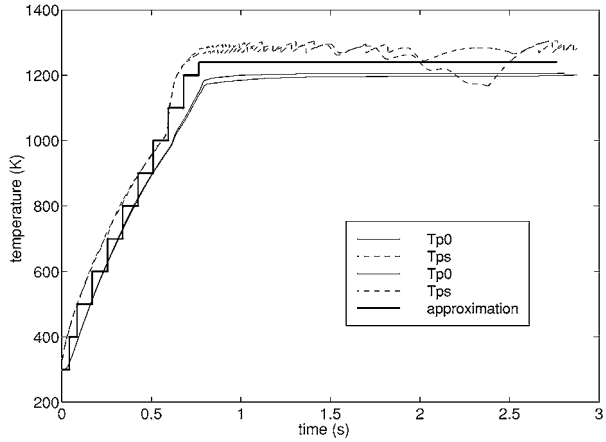

Figure 14 Typical center (Tp0) and surface temperatures (Tps) of perlite particles with 1 mm diameter in an industrial expansion furnace. Approximation of this profile by a step function for the simulation of temperature evolution of a growing bubble in the expanding material (bold solid line).

particles during their trajectories in an industrial expansion furnace [21, 39–41]. The temperature increases nearly linearly during the first 0.75 seconds, then a quasi constant temperature is attained until the exit of the particle, 2.7 seconds after its entry.

In order to simulate this temperature evolution during the particle trajectory with our adiabatic bubble growth model, we approximate it by a step function up to a mean constant temperature at the end of the trajectory. This approximation is represented on Fig. 14 by a bold line. Temperature is increased for 100 K every 0.085 s and attains after 0.765 s a constant temperature of 1240 K. This temperature is maintained until $t = 2.7$ s after the beginning of heating. The growth results obtained with the adiabatic model at each temperature step after 0.085 s, are used to initialise the following temperature step at 100 K higher temperature. The last calculation at 1240 K is maintained for 2 s in order to calculate the final bubble radius for a total residence time of 2.765 s.

In the following sections we will present the results of these simulations in function of the most important parameters which are viscosity, diffusion coefficient and water content for two different initial cell sizes ($R_0 = 4.5$ μm, $S_0 = 17.2$ μm and $R_0 = 14.4$ μm, $S_0 = 20.0$ μm).

4.2.1. Influence of the viscosity

The results of our simulations are represented on Fig. 15 in function of the temperature steps, for the two different viscosity calculation methods presented above. Mass fraction of water is 3%, the diffusion coefficient is calculated with the equation of Zhang *et al.* The bubble radius R is indicated at the end of each temperature step (after $\Delta t = 0.085$ s) with filled symbols, the cell radius S is represented with hollow symbols.

Bubble growth is very small until a temperature of 1100 K (therefore we have represented only the radius from 1000 K on). This is valid for both viscosity calculation methods and both initial radiuses. The maximum growth rate is attained during the last 2 seconds at 1240 K.

This result reflects the two stages of expansion: a first phase where vesiculation takes place and an important part of the water content is driven out without notable expansion, and a second stage, after viscosity has reached the glass transition viscosity, where the material is expanded by the remaining tenth of mass percent of water [42].

The bubble radius at the end of the trajectory after 2.7 s depends very strongly on the viscosity calculation method. The smaller viscosity of Hess and Dingwell [25] gives a final radius of 100 μm, instead of 56 μm with the method of Shaw [24]. The initial radius has no influence on the final growth result, it nearly remains the same for both cases. The shell thickness ($S - R$) is smaller in the case of Hess and Dingwell (0.2−0.3 μm). The higher viscosity of Shaw leads to a shell thickness of 0.5 μm. The expansion coefficient δ of the bubble, defined as the relation between the expanded radius S_{exp} and the initial radius S_0 of the cell, is given in the following table:

	17.2		20.0	
S_0 [μm]	S_{exp}	δ	S_{exp}	δ
Hess and Dingwell	100 μm	5.8	103 μm	5.0
Shaw	56 μm	3.3	58 μm	3.0

The values obtained with Shaw's method for the perlite considered in our case are more realistic compared

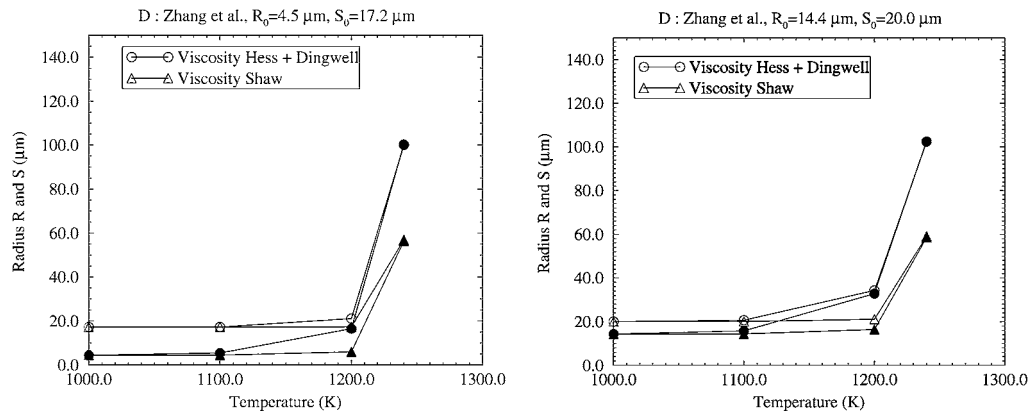

Figure 15 Influence of viscosity on bubble growth during the trajectory in an industrial furnace in function of the temperature, left: $R_0 = 4.5$ μm, $S_0 = 17.2$ μm, right: $R_0 = 14.4$ μm, $S_0 = 20$ μm; hollow symbols: evolution of S, filled symbols: evolution of R.

to industrial expansion results, where generally an expansion coefficient of 3 is obtained.

On Fig. 16, the same bubble growth case is represented in function of time. The radius at the end of each temperature step is represented by symbols. The evolution of cell radius S is represented by bold lines, the one of bubble radius R by a thin line. The rightmost symbols on the graphs indicate the radius at the furnace exit. The hypothetic growth evolution with longer residence time in the 1240 K zone is indicated by the continuing line.

Growth begins 0.85 s after beginning of heating at a temperature of 1200 K. If growth would not be interrupted after 2.7 s, the potential final radius of 122 μm would be attained at $t \approx 10$ s for the case of Hess and Dingwell, and after $t \approx 20$ s for the case of Shaw. These two results are independent of the initial bubble size.

4.2.2. Influence of the initial water content

The influence of water content on bubble growth during the particle trajectory in an expansion furnace is represented on Fig. 17 for two initial radiuses ($R_0 = 4.5$ μm, $S_0 = 17.2$ μm and $R_0 = 14.4$ μm, $S_0 = 20.0$ μm). Viscosity and diffusion coefficient are calculated with the methods of Shaw and Zhang *et al.* The rightmost symbols indicate the radius at the furnace exit. The evolution with a longer residence time is represented by a solid line.

The bubble radius at furnace exit (symbols) increases with initial water content. With 4% water content, the radius (at 2.7 s) is two times bigger than with 2% water. The shell thickness increases from 0.3 μm to 1 μm for 2% water content. The initial radius has only a small influence, at 2% water content the exit radius is 35 μm for an initial bubble of $R_0 = 4.5$ μm, instead of 40 μm for $R_0 = 14.4$ μm. Significative growth always starts at 1200 K after a heating time of about 0.85 seconds. The exit radiuses and expansion coefficients δ are represented in the following table. All values are situated in the range of industrially obtained expansion coefficients.

	17.2		20.0	
S_0 [μm]	S_{exp}	δ	S_{exp}	δ
2% H_2O	35 μm	2.0	40 μm	2.0
3% H_2O	57 μm	3.3	59 μm	3.0
4% H_2O	74 μm	4.3	74 μm	3.7

4.2.3. Influence of the diffusion coefficient

The influence of the water diffusion coefficient on the results of the trajectory simulations is represented on Fig. 18 Water content is 3%, viscosity has been calculated with the method of Shaw.

With the diffusion coefficients of Moulson and Roberts, the bubble is much smaller (29 μm) at the

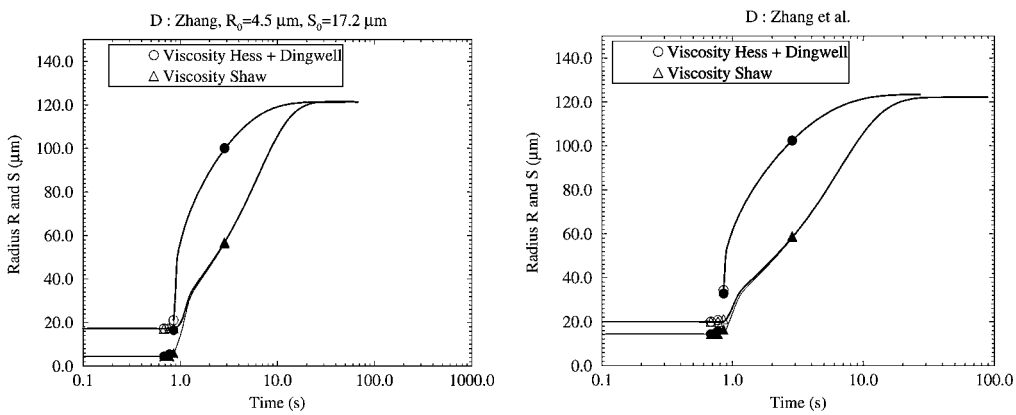

Figure 16 Influence of viscosity on bubble growth during the trajectory in an industrial furnace in function of time, left: $R_0 = 4.5$ μm, $S_0 = 17.2$ μm, right: $R_0 = 14.4$ μm, $S_0 = 20$ μm; hollow symbols: evolution of S, filled symbols: evolution of R.

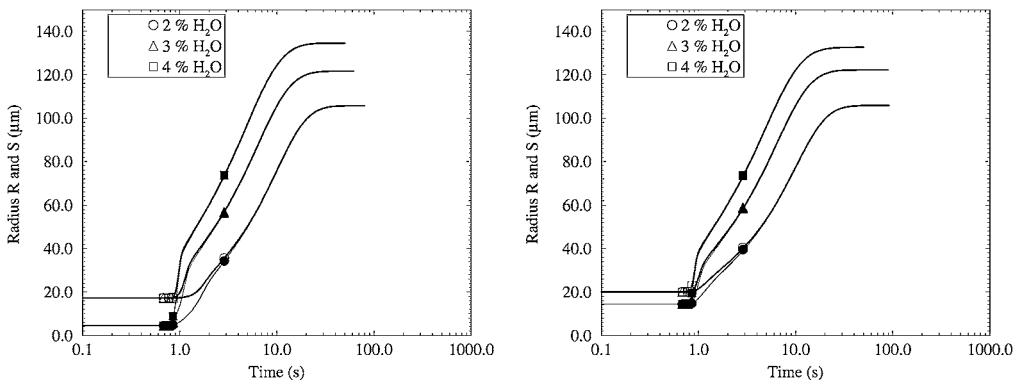

Figure 17 Influence of initial water content on bubble growth during the trajectory in an industrial furnace in function of time, left: $R_0 = 4.5$ μm, $S_0 = 17.2$ μm, right: $R_0 = 14.4$ μm, $S_0 = 20$ μm; hollow symbols: evolution of S, filled symbols: evolution of R.

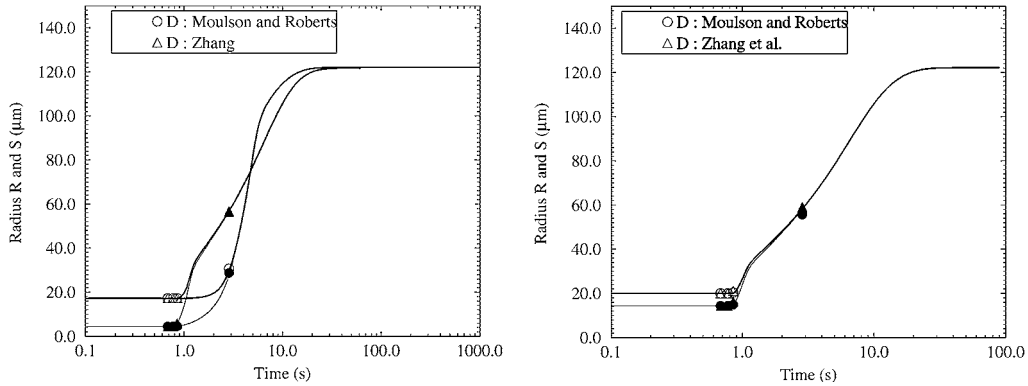

Figure 18 Influence of diffusion coefficient on bubble growth during the trajectory in an industrial furnace in function of time, left: $R_0 = 4.5\ \mu$m, $S_0 = 17.2\ \mu$m, right: $R_0 = 14.4\ \mu$m, $S_0 = 20\ \mu$m; hollow symbols: evolution of S, filled symbols: evolution of R.

furnace exit than with the coefficient of Zhang (57 μm), if starting with a cell of $S_0 = 17.2\ \mu$m (Fig. 18 left, symbols at $t = 2.7$ s). In the case of the initially bigger cell (Fig. 18 right, symbols at $t = 2.7$ s) the difference of the exit bubble radius is much smaller (58.5 μm instead of 55.6 μm). The shell thickness is 0.6 to 0.9 μm for the diffusion coefficient of Moulson and Robert, compared to 0.5 μm for the coefficient of Zhang. The expansion coefficients δ in the following table depend less on the initial size for the coefficients of Zhang *et al.* than for those of Moulson and Roberts.

	17.2		20.0	
S_0 [μm]	Sexp	δ	Sexp	δ
Moulson and Roberts	29 μm	1.7	58.5 μm	2.8
Zhang *et al.*	57 μm	3.3	55.6 μm	3.0

A bigger surface of the bubble apparently counterbalances the smaller diffusion coefficient of Moulson and Roberts, and the water mass flux is no longer determined by the diffusion coefficient, as for small bubbles, but by the bubble surface.

5. Discussion and conclusions

A bubble growth model for the simulation of perlite expansion has been developed. The numerical results obtained with this model for bubble growth in a finite volume of melt allow a better understanding of the expansion phenomenon of perlite.

The most important parameters for the process have been emphasised. They are the water content of the melt, temperature and related to those the viscosity and diffusion coefficient of water in the melt. Viscosity and diffusion coefficients are difficult to determine experimentally and literature values show very large differences concerning these parameters. Water content is intrinsic to the material used and generally cannot be determined continuously in an industrial context. The only parameter which can be changed easily in the industrial process is the temperature evolution.

The comparison of the model results with experimental values [1, 21, 43] can help us to determine a set of calculation methods for viscosity and the diffusion coefficient for the material used:

- With the method of Shaw [24] a bubble growth of about 3 times the initial radius is predicted, which corresponds to industrial perlite expansion coefficients. The method of Hess and Dingwell [25], in our case, leads to an expansion coefficient which is 5 times the initial radius, and thus too big compared to industrial values.
- The final cell size ($d = 2 \cdot S = 116\ \mu$m) obtained with the methods of Shaw (viscosity) and Zhang *et al.* [34] (diffusion) lies near experimental values determined by electron microscopy [21, 43], which are between 20 μm and 170 μm with a mean value of 80 μm. The method of Hess and Dingwell (viscosity), estimating a cell diameter of $d = 200\ \mu$m, gives too large bubbles compared to these experimental values.
- The calculation method of the diffusion coefficient has a very strong influence on the simulation results. With the method of Moulson and Roberts [33], the final bubble size depends very strongly on the initial cell size, which is not the case with the method of Zhang *et al.* The final bubble radius of 29 μm ($d = 58\ \mu$m for an initial cell size of $S_0 = 14.4\ \mu$m) is at the lower limit compared to the experimental results. The expansion coefficient of 2 is smaller than the industrial one.
- Shell thickness at the end of expansion varies in our calculations between 0.2 μm with the methods of Hess and Dingwell (viscosity) and Zhang *et al.* (diffusion), and 0.6 to 0.9 μm with the method of Shaw for viscosity. Experimental results [21, 43] give a wall thickness of 0.1 to 1 μm. The calculation results correspond very well to these values.

In conclusion of these comparisons, it seems that the combination of the viscosity calculation of Shaw [24] and the diffusion coefficient of Zhang *et al.* [34] are the most appropriate for the simulation of the expansion process of the perlite used here. The expansion coefficient and wall thickness are reproduced very well. The bubble size is slightly overestimated compared to the experimental mean value.

This overestimation can be explained by several model assumptions. In the model the bubble is impermeable at its external surface. All the water in the melt only can diffuse to the gas bubble. In reality the bubble also has water loss at its outer surface or can even crack.

Coalescence and film drainage have not been taken into account in our model. Due to the high viscosity of the melt these phenomenon should not have a strong influence on growth.

Viscosity of real perlite melt may be higher than the calculated one. Solid inclusions and micropores in the molten material can influence viscosity in such a way [44]. There are also doubts concerning the Newtonian behaviour of the melt [19], as supposed in the model.

In the calculations, expansion begins at 1100 K (830°C) with an accelerated expansion between 1200 and 1240 K (930 to 970°C). These temperatures correspond to industrial expansion temperatures and laboratory experiments concerning the kinetics of perlite expansion [42]. The calculations show the strong influence of residence time in a given temperature level and of the temperature level itself. In the industrial process, which treats inhomogeneous material, these parameters will represent the key to the desired expansion result. A slightly higher residence time can lead to a strong increase of the expansion rate.

Acknowledgements

The numerical code used in this study initially had been developed at the University of New Hampshire in the United States. The authors would like to thank Prof. Alex Proussevitch and Prof. Dork Sahagian for the transmission of their code and the numerous exchanges concerning its structure and utilisation.

References

1. K. ZÄHRINGER *et al.*, *Chemie der Erde - Geochemistry*, accepted for publication.
2. L. GIBSON and M. ASHBY, "Cellular solids, structure and properties" (Pergamon Press, 1988).
3. M. AMON and C. DENSON, *Polymer Eng. and Science* **24**(13) (1984) 1026.
4. A. AREFMANESH and S. ADVANI, *Rheologica Acta* **30** (1991) 274.
5. *Idem.*, *Polymer Eng. and Science* **35**(3) (1995) 252.
6. A. AREFMANESH, S. ADVANI and E. MICHAELIDES, *ibid.* **30**(20) (1990) 1330.
7. M. SHAFI, J. LEE and R. FLUMERFELT, *ibid.* **36**(14) (1996) 1950.
8. A. PROUSSEVITCH, D. SAHAGIAN and A. ANDERSON, *J. Geophysical Research* **98**(B12) (1993) 22.
9. R. SPARKS, *ibid.* **99**(B9) (1994) 17.
10. D. SAHAGIAN, A. PROUSSEVITCH and A. ANDERSON, *ibid.* **99**(B9) (1994) 17.
11. A. PROUSSEVITCH and D. SAHAGIAN, *ibid.* **101**(B8) (1996) 17.
12. D. SAHAGIAN and A. PROUSSEVITCH, *J. Volcanology and Geothermal. Research* **74** (1996) 19.
13. R. S. SPARKS, *ibid.* **3** (1978) 1.
14. C. W. BURNHAM, *Geochim. Cosmochim. Acta.* **39** (1975) 1077.
15. Perlite Institute INC., *Perlite Design Manual*, New York.
16. Roskill Information Services Limited, *Perlite* (1977).
17. "Ullmann's Encyclopedia of Industrial Chemistry," Vol. A23 (VCH).
18. T. MURASE and A. MCBIRNEY, *Geol. Soc. of Am. Bulletin* **84** (1973) 3563.
19. A. MCBIRNEY and T. MURASE, *Ann. Rev. Earth Planet. Science* **12** (1984) 337.
20. I. FRIEDMAN, W. LONG and R. SMITH, *Journal of Geophysical Research* **68**(24) (1963) 6523.
21. K. ZÄHRINGER, PhD Thesis, Ecole Centrale Paris (1998).
22. H. SCHOLZE, "Glass: nature, structure, and properties" (Springer Verlag, New York, 1991).
23. Y. BOTTINGA and D. WEILL, *Am. Jour. Scie.* **272** (1972) 438.
24. H. SHAW, *ibid.* **272** (1972) 870.
25. K.-U. HESS and D. DINGWELL, *American Mineralogist* **81** (1996) 1297.
26. T. MURASE and A. MCBIRNEY, *Science* **167** (1970) 1491.
27. R. STEVENSON, N. BAGDASSAROV and C. ROMANO, *Earth and Planetary Science Letters* **146** (1997) 555.
28. N. BAGDASSAROV and D. DINGWELL, *J. Volcanology and Geothermal Research* **60** (1994) 179.
29. Y. S. TOULOUKIAN (Ed.), "Thermophysical Properties of Matter" (IFI-Plenum, New-York, 1970).
30. E. KING, S. TODD and K. KELLEY, Bureau of Mines Report, R.I. 4394 (1948).
31. C. BACON, *American Journal of Science* **277** (1977) 109.
32. R. MARSHALL, *Geological Society of America Bulletin* **72** (1961) 1493.
33. A. MOULSON and J. ROBERTS, *Trans. Brit. Ceram. Soc.* **59** (1960) 388.
34. Y. ZHANG, E. STOLPER and G. WASSERBURG, *Geochimica et Cosmochimica Acta* **55** (1991) 441.
35. E. BOULOS and N. KREIDL, *Jour. Canadian Ceramic Society* **41** (1972) 83.
36. I. FRIEDMAN, R. SMITH and W. LONG, *Geological Society of America Bulletin* **77** (1966) 323.
37. R. LEE, *Physics and Chemistry of Glasses* **5**(2) (1964) 35.
38. J. KARSTEN, J. HOLLOWAY and J. DELANEY, *Earth and Planetary Science Letters* **95** (1982) 420.
39. K. ZÄHRINGER, A. KLIPFEL, J.-P. MARTIN, J.-P. PETIT and M. FOUNTI, "Experimental and computational investigation of vertical perlite expansion furnaces," 4th European Conference on Industrial Furnaces and Boilers, Porto, April 1997.
40. A. KLIPFEL, K. ZÄHRINGER, M. FOUNTI, J.-P. MARTIN and J.-P. PETIT, "Numerical simulation and experimental validation of the turbulent combustion and perlite expansion processes in an industrial perlite expansion furnace," 11th Symposium on Turbulent Shear Flows, Grenoble, France, Sept. 1997.
41. K. ZÄHRINGER, J.-P. PETIT, J.-P. MARTIN, A. KLIPFEL and M. FOUNTI, "Etude expérimentale et modélisation numérique d'un four d'expansion pour des matériaux isolants d'origine minérale," 6e Congrès Français de Génie des Procédés, Paris, Sept. 1997.
42. N. BAGDASSAROV, F. RITTER and Y. YANEV, *Glass Science and Technology* **72**(9) (1999) 277.
43. S. MERIANI and F. FONTANIVE, *Materials Chemistry* **1** (1976) 347.
44. A. BOCCACCINI, K. KIM and G. ONDRACEK, *Mat.-wiss. und Werkstofftechnik* **26** (1995) 263.

Received 10 May
and accepted 26 December 2000